Available online at website: https://journal.bcrec.id/index.php/bcrec

Bulletin of Chemical Reaction Engineering & Catalysis, 19 (1) 2024, 47-60

Research Article

The Properties and Activity of TiO_2-based Nanorods as an Anti-Fouling Agent and a Photocatalyst

Sri Wahyuni[1,*], Indriana Kartini[2], Sri Kadarwati[1]

[1]Chemistry Study Program, Faculty of Mathematics and Natural Sciences, Universitas Negeri Semarang, Semarang 50229, Indonesia.
[2]Department of Chemistry, Faculty of Mathematics and Natural Sciences, Universitas Gadjah Mada, Yogyakarta 55281, Indonesia.

Received: 14th November 2023; Revised: 27th December 2023; Accepted: 2nd January 2024
Available online: 12nd January 2024; Published regularly: April 2024

Abstract

The properties and activity of TiO_2-based nanorods as an antifouling agent and a photocatalyst for the catalytic degradation of methylene blue (MB) have been investigated. A modification of TiO_2 with SiO_2 was first carried out to enlarge the surface area. In order to enhance the TiO_2 photo response to the visible light region, a further modification of TiO_2-SiO_2 (TS) composites with polyaniline (PANI) was also conducted. The nanorod TiO_2 exhibited an anatase structure based on the diffraction patterns. The TEM images showed that some TiO_2 molecules were attached around SiO_2 with a random orientation. The TiO_2-SiO_2-PANI (TS-PANI) exhibited the largest specific surface area (S_{BET}) of about 256.85 m^2/g. The profile on the AFM images of the composites showed that the nano-roughness of the coatings was confirmed. The photocatalytic activity was evaluated through the degradation of MB both on the powder and the coated composites. The photocatalytic activity on the coatings was verified due to further application as anti-fouling coatings involving photocatalytic mechanism. The degradation of MB using TS-PANI powder and TS-PANI coating composites was 89.5% and 90.2%, respectively, with the irradiation time on the coatings was 20 min longer. The anti-fouling activity through the photocatalytic mechanism and nano-roughness surface was confirmed by the inhibition of barnacle growth on the teakwood surface immersed for two months in the sea.

Keywords: TiO_2; Polyaniline; Coating; Photo-Activity; Anti-Fouling Agent

How to Cite: S. Wahyuni, I. Kartini, S. Kadarwati (2024). The Properties and Activity of TiO_2-based Nanorods as an Anti-Fouling Agent and a Photocatalyst. *Bulletin of Chemical Reaction Engineering & Catalysis*, 19 (1), 47-60 (doi: 10.9767/bcrec.20074)

Permalink/DOI: https://doi.org/10.9767/bcrec.20074

1. Introduction

The technology of wastewater treatment has been continuously developed to achieve an effective and efficient method to remove the pollutants from the aquatic environment. The removal of dyes, especially methylene blue as a primary dye, from wastewater have been intensively investigated due to its high toxicity and non-biodegradable property [1]. Various methods of dyes-containing wastewater treatment, such as adsorption [2], precipitation [3], ultra-filtration [4] and coagulation [5] have been studied. The photocatalytic degradation of dyes using a photocatalyst has been considered as the most advantageous method [6]. It could convert the organic pollutants into smaller and safer molecules to be disposed to the environment.

Investigation and development of TiO_2 are increasingly beneficial due to its wide application, especially as a photocatalyst. TiO_2 photocatalyst used in a variety of applications and products in the environmental and energy fields, including self-cleaning surfaces [7], air and water purification systems, hydrogen evolution [8,9], sterilization [10], and wastewater treatment [11]. TiO_2 extensively studied due to its strong

* Corresponding Author.
Email: sriwahyunikimia@mail.unnes.ac.id (S. Wahyuni);
Telp: +62-24-8508035, Fax: +62-24-8508035

oxidation ability to decompose various organic pollutants [7,8], excellent chemical stability, long durability, and nontoxic [10,12]. TiO_2 also widely developed as an active agent for anti-fogging [12], self-cleaning coating [13], and an anti-fouling coating [14,15]. Several characteristics of TiO_2 as a photocatalyst, such as surface area, crystallinity, morphology, crystalline phase, and photo-response, considered as important factors affecting its performance.

Biofouling is considered a serious problem in the marine life. Biofouling is the accumulation of living organisms on a ship's surface that begins by attachment of microorganism. First, a layer consisting of organic substances, such as proteins or polysaccharides, were formed on the surface of the substrate and then triggers the adhesion of subsequent microorganisms to form a biofilm. This biofilm then develops into an adverse fouling layer [16]. One of the safe ways to control the fouling is to use a photocatalyst that act to inhibit the formation of biofilms through a photocatalytic mechanism [17,18]. As a photocatalyst, TiO_2 acts to inhibit the micro-foulant growth or biofilms on the surface material like boats or ships [19,20]. In recent years, TiO_2 with a nanorod morphology was studied as an active material in a self-cleaning coating [21]. Several studies reported that as a coating, the TiO_2 nanorods provide a nano-roughness on the surface and act to inhibit the fouling attachment or biofilms formation. Therefore, the TiO_2 nanorods are very potential to perform nano-roughness on the surface and inhibit the attachment of biofilms or foulants by a photocatalytic mechanism.

Supporting TiO_2 on a thermally stable material such as SiO_2 would improve its properties, especially the surface area, pore-volume, and pore diameter [22,23] while reducing the susceptibility of agglomeration. The improvement of these properties will be able to increase the photocatalytic activity of TiO_2-SiO_2 [23–25]. In the coating application, SiO_2-modified Ti provided a lower surface energy and better hydrophobic property to the coating films [26–28]. The initial layer of fouling is a layer of bacteria that will be decomposed by free radicals formed because TiO_2 absorbs the appropriate photons. In addition, SiO_2 in coatings produces better layer surfaces and reduces biofilm adhesion. The TiO_2-SiO_2 composites were also expected to form a homogeneous layer when dispersed in an acrylic matrix for coatings as has been reported earlier [17,29]. Therefore, a better activity would be observed in the SiO_2-combined TiO_2 for an anti-fouling coating.

In addition to the activity as an antifouling coating, the improvement of the photo response of TiO_2 to the visible light areas is important to study. Adding conductive polymers such as polyaniline (PANI), polythiophene, and poly-pyrrole played an important role as a sensitizer to increase the photo-response of TiO_2 to the visible regions [30–35]. PANI itself has been considered as a useful modifier to improve the photo-response of TiO_2 because it is easy to synthesize and provide benefits in marine coating [20,32].

It was reported that the photocatalytic performance of TiO_2-SiO_2-PANI was quite low due to the high amount of PANI added in the composites [36]. In this study, the TiO_2-SiO_2/PANI composites were synthesized using a solvothermal method with reduced amount of PANI in order to develop the photocatalysts with a better characteristic and performance. The performance of the composites was evaluated through the photocatalytic degradation of methylene blue and as a coating to prevent the fouling attachment over time. The kinetics of the photocatalytic activity of the TiO_2-SiO_2/PANI composites in the forms (powder and coating) was studied. In addition, the anti-fouling activity of the composites was also investigated using iron teak wood plates immersed in Tanjung Emas port for two months.

2. Materials and Methods

2.1 Materials

Titanium tetra-isopropoxide (TTiP, 97%) Na_2EDTA (99%) purchased from Sigma Aldrich was used as the precursor of Ti and Ti growth directing agent, respectively. Ammonia (28%, E. Merck), toluene (99.5%, Mallinckrodt), and demineralized water were used for the preparation of TiO_2 nanorods. Tetraethyl orthosilicate (TEOS, 99%) and ethanol (99.5%) were all from E. Merck and used during the preparation of SiO_2. Acetic acid (CH_3COOH, 99.8%) was from E. Merck and used for the synthesis of TiO_2–SiO_2 composites. Ammonium peroxy-disulfate (APS, 98%), aniline (99.5%), and HCl (37%), all from E. Merck, were used for the synthesis of TiO_2–SiO_2–PANI. Aniline first distilled under a low pressure of about 0.8 atm prior its use.

2.2 Synthesis of TiO_2-SiO_2/PANI Composites

The first stage of this study was the synthesis of TiO_2 nanorods and SiO_2. The synthesis of TiO_2 nanorods was carried out by the solvothermal method [37]. The process was started by slowly (in dropwise), adding 5 mL of TTiP into 25 mL of 0.2 M Na_2EDTA solution. Together with the process, 50 mL of toluene was also added slowly into Na_2EDTA solution. The mixture was stirred using a magnetic stirring system, then transferred into an autoclave, and heated at 180 °C for 3 h. The precipitate obtained was dried at 70 °C for 6 h.

The synthesis of SiO_2 was carried out by a modified sol-gel method, as was reported earlier

[38]. TEOS, NH_3, ethanol, and demineralized water were prepared in the following volume ratio (in mL): TEOS : ethanol : NH_3 : demineralized water = 9 : 8 : 6.5 : 26.5. TEOS was dissolved in ethanol and stirred using a magnetic stirrer for 30 min. NH_3 and demineralized water then were added dropwise while stirring for 2 h. The precipitate obtained was filtered and washed till neutral and dried in an oven at 60 °C for 24 h.

TiO_2-SiO_2 composites (hereinafter referred to as TS) were prepared in accordance with the hetero-coagulation method proposed by Wilhelm [33]. One gram of SiO_2 was dispersed into demineralized water, and the pH was adjusted to 7.5-8 by adding concentrated NH_3. Meanwhile, 0.428 g of TiO_2 nanorods was dispersed into demineralized water, and the pH was adjusted to 2-3 by adding concentrated CH_3COOH. The obtained suspension was sonicated for 1.5 h. During this process, the suspension of TiO_2 nanorods was slowly added into the SiO_2 suspension. Then the mixture of the suspensions was aged for 24 h after sonication. The precipitate was separated by a 400-rpm centrifugation and then dried in an oven at 70 °C for 12 h. The precipitate obtained was then calcined at 500 °C for 3 h. The same procedure was conducted for other amounts of TiO_2 of 0.43, 1.00, and 2.33 g. The obtained material from this step attributed to TS-30, TS-50, and TS-70 composites. These composites underwent the measurement of specific surface area, and the results were used as the consideration of which composite would be used for the preparation of TS-PANI composites.

The TS composite showing the highest specific surface area was then combined with PANI to form the TS-PANI composites. The TS-PANI composites were synthesized by a set of the ratios of the TS composites to aniline using a method as was previously reported by Li [23]. One gram of TS powder was dispersed into 80 mL of 1 M HCl solution, then homogenized by ultrasonic irradiation for 20 min. The suspension was added with 0.05 mL of aniline under a continuous ultrasonic irradiation. The APS solution in HCl was added dropwise into the mixture while continuing the irradiation for 4 h (the mole ratio of aniline to APS was 1:1.15) [30]. The composites obtained were washed until the pH reached 7 and then dried at 70 °C for 12 h. The composites obtained were labelled as TS-PANI composites.

The next process was dispersing the composites into an acrylic resin to form a coating composite. The dispersion of TS and TS-PANI composites into the acrylic resin was performed as follows. A 0.1545 g of each composite was suspended in 5 mL of demineralized water. The suspension was then added to 5 g of acrylic resin and stirred until homogeneous. The coating composite was then manually coated onto a plate surface (3 x 3 cm) using an applicator and allowed to dry [40,41]. The photocatalytic activity of the powder and coating composites of TS and TS-PANI was studied through MB degradation in an aqueous solution. In addition, the anti-fouling activity of the TS and TS-PANI coating composites was also examined.

2.3 The Characterization of the Composites

The XRD analysis was carried out on the powder TiO_2 nanorods, TS composites, TS-PANI composites, and the coating composites. The diffraction patterns were obtained on a Rigaku Mini-flex 600 X-ray diffractometer using Cu Kα (λ of 0.15418 nm) radiation with an Ni filter at 45 kV and 20 mA in the range of 2θ of 10-80°. In addition, a double beam Shimadzu 2450 diffuse reflectance UV spectrometer and a Shimadzu FTIR-820 IPC spectrophotometer were used to evaluate the band-gap energy and the functionalities of the synthesized materials, respectively.

An analysis to confirm the morphology of TiO_2 and its composites was also carried out using a JEOL JEM-1400 TEM instrument with an accelerating voltage of 40-120 kV. The surface properties of the composites, i.e. S_{BET}, pore-volume, and pore diameter, were determined through the BET method using a Nova 3200e Quantachrome surface area analyzer. Moreover, the interaction between components in the composites was studied using a high-resolution Auger electron spectrometer (X-ray Photoelectron Spectroscopy - XPS) equipping a Kratos/Axis Ultra DLD atomic emission-X ray photoelectron spectrometer with a detection limit of 0.1-1% atom. The topography of the coating was analyzed using a Park System XE-70 non-contact-type atomic force microscope.

2.4 The Evaluation of the Photocatalytic and Anti-fouling Activity

The photocatalytic activity of TS and TS-PANI composites was evaluated through the degradation of methylene blue (MB) using a light emitting diode lamp irradiation with a λ of 550-590 nm. Moreover, the photocatalytic activity of the composites coated on the surface of the plate was also studied.

In each experiment, a 100 mL of 10 ppm MB solution and 100 mg of TiO_2 nanorod, TiO_2–SiO_2 (TS), and TS–PANI composites were mixed and homogenized in a sonication bath for 15 min. The mixture was then left in the dark condition for 30 min until the adsorption-desorption equilibrium was reached. The mixture was sequently exposed to visible light using a Philips LED 120 watt for 100 min under a constant magnetic stirring of 500 rpm. A 2 mL of MB solution was taken every 20 min during the visible light irradiation. The

possible solid was separated through centrifugation. The concentration of MB solution was quantified using a mini 1240 Shimadzu UV-Vis spectrophotometer at a wavelength of 663-664 nm. The percentage of degraded MB through the photocatalytic degradation using the materials synthesized in this study was determined using Equation (1), where C_0 and C_t are the initial concentration of MB solution and after time t.

$$\%Degraded\ MB = \frac{C_0 - C_t}{C_0} \times 100\% \quad (1)$$

In addition to the photocatalytic activity, the anti-fouling activity of the composites coated on the surface of the teak wood with a size of 10 x 15 cm was also investigated. The surface of the teak wood plate was first coated with the coating composites. The plate then was dipped in the seawater at Tanjung Emas Port, Central Java, Indonesia with a depth of about 1 m. The change on the surface then observed every week for two months to inspect the growth of the sticking barnacle (one of the foulants) that most often appears on the surface of the plate.

2.5 Kinetic Study

The kinetics of the photocatalytic degradation of MB using TiO_2, TS composites and TS-PANI powder and coating composites was studied using a pseudo-first order kinetics equation, as presented by Equations (2) and (3). C_0 and C_t are the initial concentration and that after the photocatalytic degradation of MB solution, respectively, at a specific time t. This kinetics equation was selected after the linear profile of the photocatalytic degradation of MB solution was obtained. The activity of TiO_2 nanorod, TS, and TS-PANI photocatalysts was evaluated by comparing the k_{app} value obtained from the plot $\ln(C_0/C_t)$ against time (t).

$$-\ln\left(\frac{C_t}{C_0}\right) = k_{app}t \quad (2)$$

$$\ln\left(\frac{C_0}{C_t}\right) = k_{app}t \quad (3)$$

3. Results and Discussion

3.1 XRD and TEM Analyses

The synthesis of the TiO_2 nanorods through the solvothermal method resulted in a crystal powder with a length of about 40-50 nm and a diameter of about 10-15 nm confirmed from the TEM images of TiO_2 nanorods, SiO_2, TS composite, and TS-PANI composites in Figure 1. The TEM images confirmed that the similar size of the TiO_2 rod was observed, although some aggregation still formed. The shape of the TiO_2 nanorods looked elongated with a pointed tip. A similar shape of the rod TiO_2 has also obtained by Baek *et al.* [42] and Chemseddine [43]. The existence of SiO_2 was also detected in Figure 1, with a diameter of about 200-250 nm.

The crystallinity of the TiO_2 nanorods and the composites was confirmed from the diffraction patterns shown in Figure 2. The diffraction patterns in Figure 2 confirmed that TiO_2 with the anatase phase was obtained in accordance with the standard data of JCPDS number 00-021-1272. The orientation of crystal growth was determined by calculating the textural coefficient (TC) values from the X-ray diffraction data [44,45]. If the TC values for all planes (*hkl*) approaches one, the crystal growth orientation of the particles would be

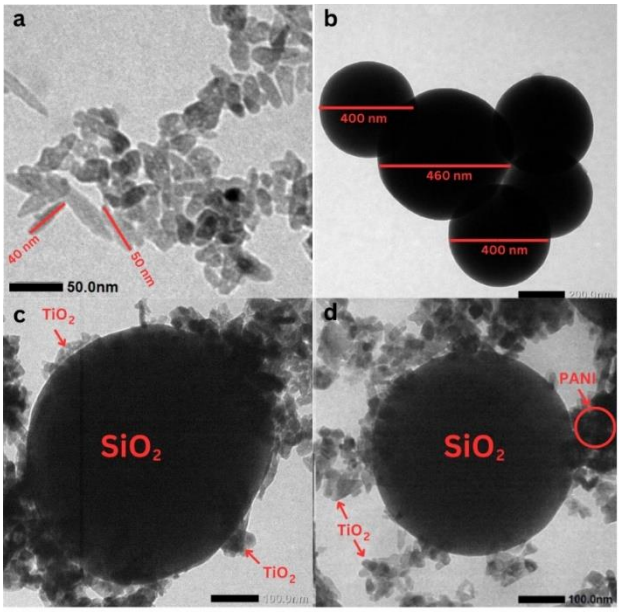

Figure 1. The TEM images of (a) TiO_2 nanorods, (b) SiO_2, (c) TS, (d) TS-PANI composites.

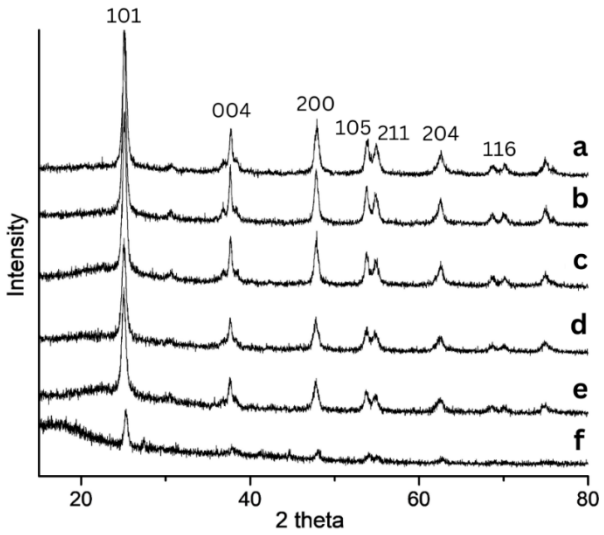

Figure 2. Diffraction patterns of (a) TiO_2, (b) TS-70, (c) TS-50, (d) TS-30, (e) TS-PANI composites, and (f) the coating TS-PANI composites.

randomly approached the JCPDS standard as a reference. However, if several of the TC values is greater than 1, the abundance of the crystal grains is formed in a certain direction [40]. The textural coefficient of (004) planes in TiO_2 was 1.27. Moreover, the (101), (105), (204), and (215) planes showed a TC value of 0.77, 1.01, 1.05, and 1.15, respectively. These TC values indicated that the growth of TiO_2 crystals in this study has occurred in one certain direction, even though these values was not as high as those for the material grown directly on the surface of a substrate as reported earlier [45,47].

This study also showed that by increasing the amount of TiO_2 added in the TiO_2-SiO_2 composites (labeled as TS-30, TS-50, and TS-70) and even with the addition of PANI in the coating composites, the anatase phase was consistently observed. A decrease in the intensity of the diffraction patterns was also observed, possibly due to the inclusion of SiO_2 in the TiO_2 crystal lattice. The TiO_2 with anatase phase has been considered as the most responsible phase for the photocatalytic activity of TiO_2 through the degradation of the undesirable organic compounds in the environment. The decrease in the intensity of anatase was quite dramatic after the composites being mixed with acrylic binders when the composite applied in the coating. In the coating-composites, the concentration of composites added was only 3% of the weight of the acrylic resin. Therefore, a significant decrease in the intensity of the diffraction patterns was observed (Figure 2(f)).

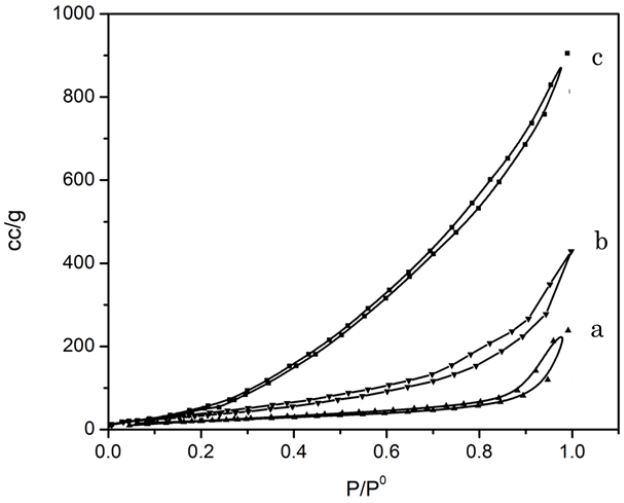

Figure 3. The N_2 adsorption-desorption curve of (a) TiO_2, (b) TS, and (c) TS-PANI composites.

3.2 N_2 Adsorption-Desorption Analysis

In addition to the crystallinity, another important characteristic required by a photocatalyst, including TiO_2, is the surface properties. A change of the surface properties of TiO_2 was observed due to the addition of SiO_2 and PANI in the TS and TS-PANI composites. These changes could be revealed through a porosity analysis, specifically through the nitrogen adsorption-desorption (Figure 3) for TiO_2, TS composite, and TS-PANI composite. The differences of the curve shapes indicated the change in the porosity characteristics when a mixture of oxides was formed as the result of the formation of TiO_2–SiO_2 composites. The type of adsorption-desorption curve of TiO_2, TS composite, and TS-PANI composite according to International Union of Pure and Applied Chemistry (IUPAC) was the curve of type IV with hysteresis loop type H1 at a relative pressure of around 0.8. This indicated that the pore morphology of the composites was predicted as evenly distributed and cylinder-like shaped channels [48].

The porosity analysis could be also presented quantitatively as textural properties as is presented in Table 1. The TS-50 composite showed the best improvement in the surface properties compared to other composites (TS-30 and TS-70). The addition of SiO_2 to TiO_2 to form TS composites resulted in a more homogeneous structure as indicated by the increase in the specific surface area (S_{BET}). However, a slight decrease in the surface area of the TS-70 composite was observed. It was possibly due to the change in the distribution of TiO_2 layers at the SiO_2 surface. The amount of TiO_2 nanorod added in the TS-70 composite was higher, resulting in the distribution inhomogeneity of TiO_2 at the SiO_2 surface. This was possibly caused by the difficulty of the rod morphology to form a homogeneous layer at the surface of other components, such as SiO_2, as is also presented by the TEM images (Figure 1(c)).

Table 1. Textural property of TiO_2 nanorod, SiO_2, TS, and TS-PANI composites.

The composites	S_{BET} (m^2/g)	D_p (nm)	V_p (cm^3/g)
TiO_2	64.0	3.40	0.349
TS-30	58.1	12.56	0.205
TS-50 (TS)	80.4	3.28	0.246
TS-70	75.9	3.01	0.309
SiO_2	48.2	12.15	0.131
TS-PANI	256.8	3.64	1.572

A further increase in the S_{BET} was shown by the TS-PANI composites from 80.4 m^2/g in the TS-50 composite (then labelled as TS) to 256.85 m^2/g in the TS-50-PANI (then labelled as TS-PANI). The increase in the surface area was probably due to changes in the pore shape of the composites as observed in the isotherm curve (Figure 3). The pore shapes like sheets or layers would increase in the narrow slit-shaped pores [49–51].

3.3 FTIR Spectroscopy and XPS Analysis

The formation of the composites between TiO_2 and SiO_2, as well as TiO_2, SiO_2, and PANI caused changes in the chemical bonds in TiO_2 alone, as indicated by the change of peak in the IR spectra in Figure 4. The change in the chemical bonds of TiO_2 could be observed by the formation of C=N and C–N bonds in the TS and TS-PANI composites in Figure 4(b-e). In addition, the increase in the peak designated as N–H bonds in the composites was also an indication of the change in the chemical bonds in TiO_2.

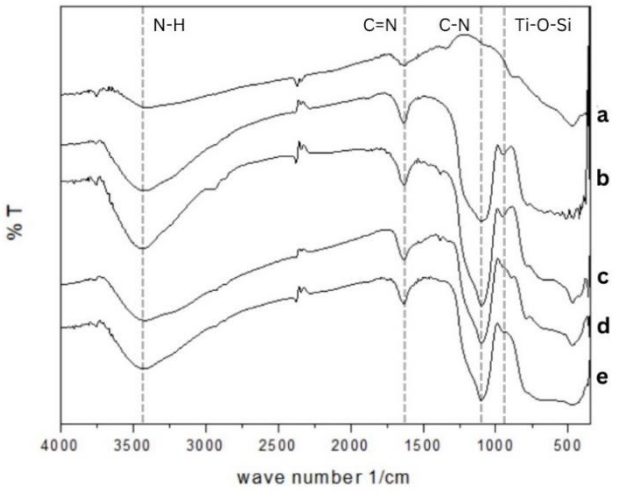

Figure 4. The FTIR spectra of (a) TiO_2, (b) TS-50, (c) TS-50-PANI, (d) TS-70, and (e) TS-70-PANI.

The interaction between TiO_2, SiO_2, and PANI in the composites was also analyzed through XPS analysis as is presented in Figure 5. On the wide spectra for the TiO_2 nanorods, peaks were occurred at 458.8 eV for Ti(2p), 529.8 eV for O(1s), and 284.6 eV for C(1s). The binding energy values calibrated with a standard value of C(1s) of 284.6 eV [52]. The binding energy of TiO_2 matched with the literature that specifically determines the characteristics of TiO_2 through XPS analysis [53]. According to the literature, the binding energy of Ti($2p^{3/2}$) was 458.15 eV base on the calculation using the standard C(1s) 284.6 eV. The binding energy of the O(1s) in TiO_2 is 529.41 eV. For TS (TiO_2-SiO_2) composites, several peaks were appeared in the wide spectrum, there were C(1s), O(1s), Ti(2p), and Si(2p) at binding energy positions of 284.25 eV, 529.25 eV, 457.25 eV, and 103.25 eV, respectively. In the spectrum of each atom, the signal of C(1s) occurred at position of 284.6 eV, while the signals of O(1s) occurred in two positions, at 529.6 eV confirmed as the Ti–O bond in TiO_2 [45]; and 533.0 eV identified as OHt–O–Ti^{4+} [54]. Meanwhile, the signals of Ti(2p) occurred at 458.3 and 464.3 eV. These values

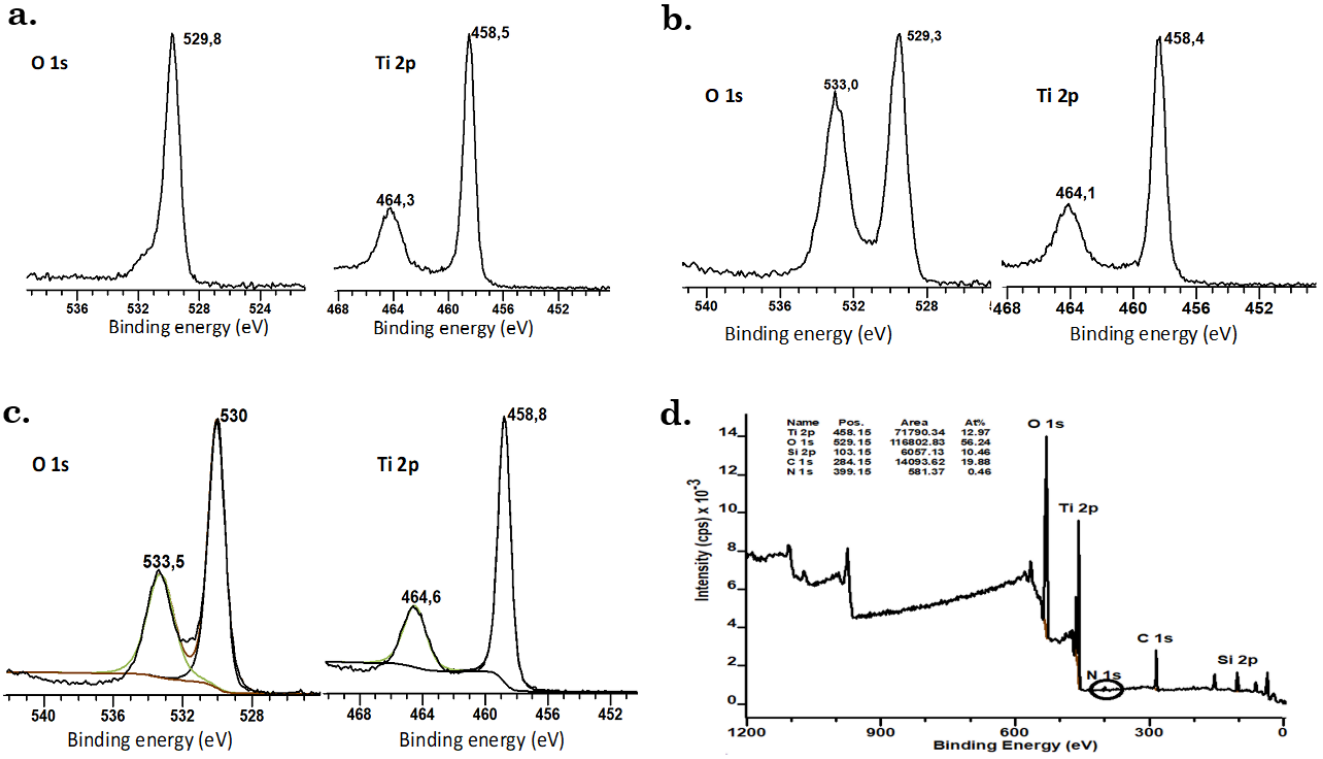

Figure 5. XPS spectra of TiO_2-SiO_2 nanocomposites: (a) binding energy position of Ti(2p) and O(1s) (as-prepared TiO_2); (b) binding energy of Ti(2p) and O(1s) of TiO_2-SiO_2 composites (c) binding energy of Ti(2p) and O(1s) of TiO_2-SiO_2-PANI composites; (d) the wide spectra of TiO_2-SiO_2-PANI composites.

shifted to the lower level than the binding energy of Ti(2p) in the TiO_2 nanorods. The shifting of the binding energy occurred due to the formation of Ti−O−Si bonds due to the inclusion of Si into the TiO_2 framework causing a shifting in electron density and further resulted in the change in the binding energy. The changes in binding energy at Ti−O can also be confirmed by observing a shift in the binding energy of O(1s) (Figure 5). Similar shifts were also reported by Wang and Zeng in their study [55].

The wide spectrum of the TS-PANI composites (Figure 5(d)) represented all the peaks of components in one frame according to the atomic fraction. The amount of N atoms in the TS-PANI composites was too small (less than one percent). Consequently, the peak of N(1s) (marked with a circle) that appeared in the wide-spectra was almost unclear. Figure 5(d) has confirmed the presence of the main components in TS-PANI composites, i.e., carbon, oxygen, titanium, silicon, and nitrogen. Those five components, C(1s), O(1s), Ti(2p), Si(2p), and N(1s) corresponded to the binding energy at 284.6, 529.8, 458.8, 103.8, and 399.8 eV, respectively. These results indicated that PANI has partially been coated on the surface of the TS composites after the aniline polymerization took place. The binding energy of N(1s) observed at 399.8 eV indicated the presence of interaction between TS composite and PANI. This binding energy was in the range of the binding energy of N−H (399-400 eV) [46,57].

3.4 Measurement of Band-Gap Energy

The light absorption ability of the synthesized materials TiO_2 nanorod and its composites with SiO_2 and SiO_2–PANI was evaluated and analyzed. The band-gap energy of the synthesized materials was determined based on the edge wavelength (λ_{edge}) and listed in Table 2. A slight change in the light absorption ability of the TiO_2 nanorod and TS composites was observed. The addition of PANI in the TS composites showed a significant decrease in the band-gap energy and the light absorption ability of TS-PANI composites has shifted to the visible range.

3.5 Photocatalytic Activity Test

The photocatalytic activity of TiO_2 nanorods, TS, and TS-PANI composites was evaluated by monitoring the decrease in the concentration of methylene blue (MB) in an aqueous solution. This experiment also used a commercial TiO_2 (available in the lab) in the photocatalytic activity test for a comparison.

The addition of different amount of SiO_2 in the TS composites gave a positive effect on the photocatalytic activity of TiO_2 during the degradation of MB, as is presented in Figure 6. The commercial TiO_2 showed the lowest activity of MB degradation. By increasing the amount of

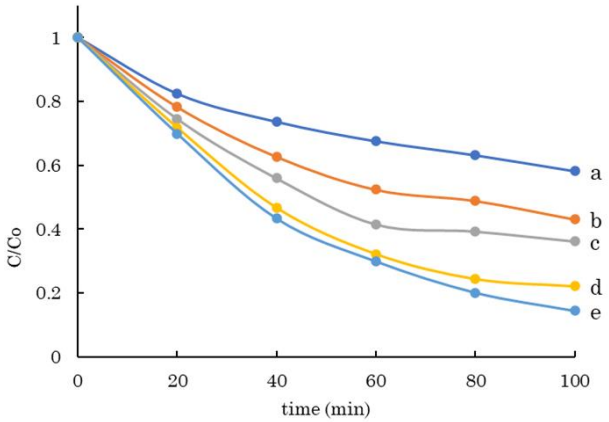

Figure 6. The decreased of MB concentration using (a) commercial TiO_2 (by Merck), (b) the synthesized TiO_2, (c) TS-30, (d) TS-50, and (e) TS-70.

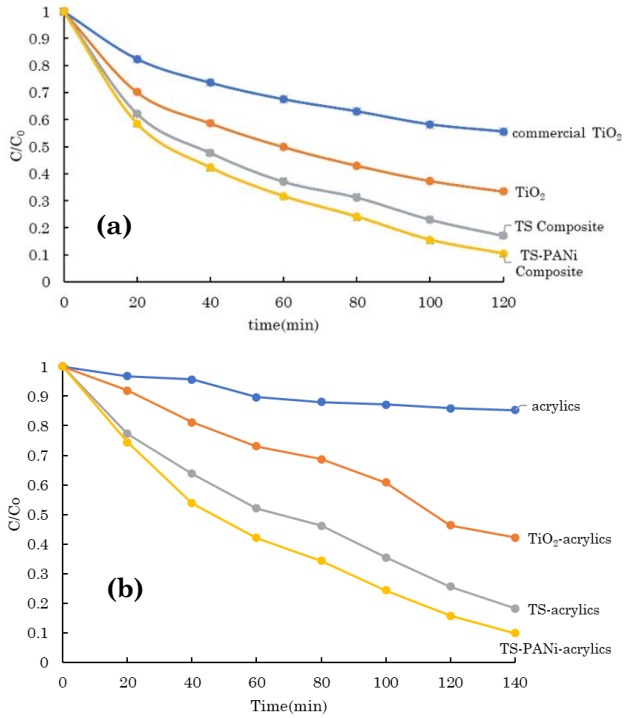

Figure 7. The decreased of MB concentration by (a) powder composites and (b) the coating composites.

Table 2. The band-gap energy of TiO_2 nanorod, TS composites and TS-PANI composites.

Sample	TiO_2	TS composites			TS-PANI composites		PANI
		TS	TS-50	TS-70	TSP-50	TSP-70	
Band-gap (eV)	3.15	3.14	3.13	3.17	2.97	3.06	2.88
λ_{edge} (nm)	394	393	396	391	418	412	431

added SiO_2 in the TS composites, the significant increase in the degraded MB was observed. TS-50 and TS-70 composites showed a similar photocatalytic activity; only a slight difference could be observed (see Figure 6). The presence of SiO_2 in the TS composites seemed promote a better electron-hole pair production to produce active to radicals to further react with the organic pollutant. Due to the better surface porosity of TS-50 composite, this composite was selected to be further investigated its activity through the formation of the powder and coating TS-PANI.

The photocatalytic activity of the TiO_2–based composites (TiO_2, TS and TS-PANI composites) in the form of powder solid and coating solid was also evaluated during the degradation of MB solution under visible light irradiation. The degradation efficiency for both forms is presented in Figure 7. The TS and TS-PANI powder composites degraded the MB solution faster than the nanorod TiO_2 and commercial TiO_2 reached (Figure 7(a)). The TS-PANI composite exhibited the best performance compared to other composites in this study. The percentage of MB solution degraded by TS and TS-PANI composites was 82.97% and 89.53%, respectively. Meanwhile, nanorod TiO_2 and commercial TiO_2 degraded the MB solution only 66.54 and 44.53%, respectively. The photocatalytic activity shown by the TS-PANI composite was 6.56%; higher than that reached by the TS composite.

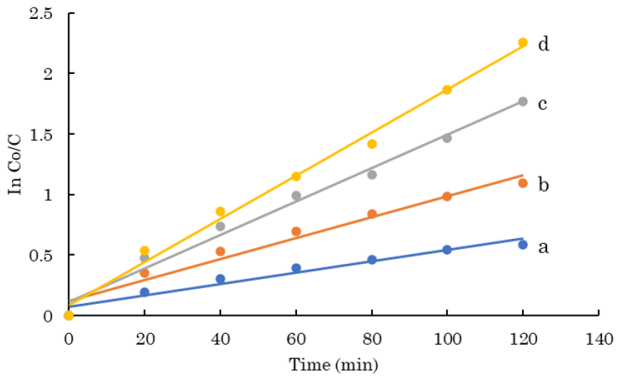

Figure 8. Fitted curves of the experimental data using a pseudo-first order kinetics equation during the photodegradation of methylene blue using (a) commercial TiO_2 (by Merck), (b) TiO_2 nanorods, (c) TS composite, and (d) TS-PANI composite.

A similar study reported that the photocatalytic activity of $Fe_3O_4/SiO_2/TiO_2$/PANI composite degraded MB solution by about 40% within a 300 minutes irradiation. The study also found that a relatively small difference in the photocatalytic activity between $Fe_3O_4/SiO_2/TiO_2$ and $Fe_3O_4/SiO_2/TiO_2$/PANI was observed [51]. Another study investigating the effect of PANI layer on TiO_2/SiO_2 composite has reported that the thickness of the PANI layer on the composite affected its photocatalytic activity. A thin PANI layer on the composite produced a higher photo-response than the thick one. On the opposite, a thick PANI layer on the composite decreased the transfer rate of charged species in the electronic state; consequently, it decreased the activity of the composites [59].

The adsorption capacity of TS and TS-PANI composites was better than that of the TiO_2 nanorod alone; this was confirmed before irradiation process on the composites. The adsorption process was run for 20 min in the dark room. The increasing of adsorption capacity may be due to the increase in the homogeneity of the composites compared to TiO_2 nanorods alone. Thus, the increase in the adsorption capacity was followed by the significant increase in the photocatalytic activity of the composite. The reaction kinetics data in Figure 8 and Table 3 showed that TS-PANI composites exhibited the highest adsorption capacity to adsorb MB until 41.39% before irradiation. This adsorption capacity was higher than that of TS composite and TiO_2 nanorods. The increase in the adsorption capacity was followed by the increase in the surface properties, especially the porosity. A better adsorption capacity provided more benefits the degradation of the dyes in the solution.

TS-PANI composites overall showed the best photocatalytic activity due to their best characteristics such as the response to light, surface area and band-gap energy, in comparison with other materials synthesized in this study. However, the addition of PANI in large amount could result in the lower photocatalytic activity. The less thick the PANI layer, the higher the photocatalytic activity. It is possibly because the thin layer of TS-PANI composite would better initiate the electron transition from the valence band to the conduction band. In addition, the thin

Table 3. The kinetics during the degradation of MB by TiO_2, TS, and TS-PANI composites.

Photocatalysts	k (min^{-1})	R^2	degraded MB after 120 min (%)	Adsorbed MB during 20 min in darkness (%)
TiO_2 (commercial)	0.0047	0.9530	44.43	17.56
TiO_2 nanorod	0.0087	0.9648	66.54	29.82
TS composite	0.0138	0.9853	82.97	37.78
TS-PANI composite	0.0178	0.9920	89.53	41.39

TS-PANI composite would not prevent the interaction between light and the TiO_2 surface.

The same experiments were also carried out to evaluate the photocatalytic activity of the coating composites as in the powder composite. The composite-acrylic coating on the surface of a 3 x 3 cm^2 plate was dipped in an MB solution and irradiated with visible light (LED Phillips 120 W). The curve of the decrease in the concentration of MB solution presented in Figure 7b. The fitted curve of the kinetic data during the MB degradation is presented in Figure 9, while the kinetic parameters are shown in Table 4. Overall, the decrease of MB solution both on the coating plate and the powder composites was almost the same. Before irradiation, the sample was placed in a dark place for 20 min to allow the adsorption took place. The amount of MB adsorbed on the plate was lower than that adsorbed in the powder composite. The photocatalytic activity test of the coating composite showed the best results on TS-PANI-acrylic with a percentage of degraded MB solution reached 90.22%.

Similar study has reported the photocatalytic activity of the coating of TiO_2(P25)-SiO_2-acrylic during the degradation of rhodamine-B [17]. The study obtained that the performance of TiO_2(P25)-acrylic coating was better than the activity of TiO_2(P25)-SiO_2-acrylic coating [17]. Other study also reported that the photocatalytic activity of TiO_2-fluoro silane-acrylic coating showed a better performance than TiO_2-acrylic coating [18]. In this study, the performance of the photocatalytic activity on TS-acrylic and TS-PANI-acrylic coatings were better than TiO_2-acrylic coating alone. It was possibly due to the composite formation between SiO_2 and TiO_2 nanorods before it was blended with acrylic. Synthesis of TiO_2-SiO_2 composites prior to coating aims to reduce agglomeration of TiO_2 and increase the surface area. Then, acrylic-composite coating still showed photocatalytic activity as evidenced by a decrease in the MB concentration.

The plausible mechanism of MB degradation using TS-PANI composites as a photocatalyst is illustrated in Figure 10. PANI molecules would cover the surface of TiO_2 and absorb the photon energy from visible light irradiation. This would allow the initiation of electron transition from the highest occupied molecular orbital (HOMO) to the lowest unoccupied molecular orbital (LUMO). The electron from PANI molecules would efficiently move to the conduction band of TiO_2 nanorod. Meanwhile, the positively-charged species (hole, h^+) would be formed. The electron transfer would take place easier between PANI molecules and TiO_2 nanorod due to the increase in the photo-response of TiO_2 nanorod with the addition of PANI.

The kinetic study of the photodegradation of MB using acrylic-coated TiO_2 and its composites (Table 4) indicated that the photocatalyst materials still showed a considerable activity on the MB photodegradation. The dispersion of TiO_2 nanorod, TS composites and TS-PANI composites in acrylic during the coating material preparation did not lead to a significant decrease of the activity of the photocatalysts. This was used as the consideration of the application of the coating

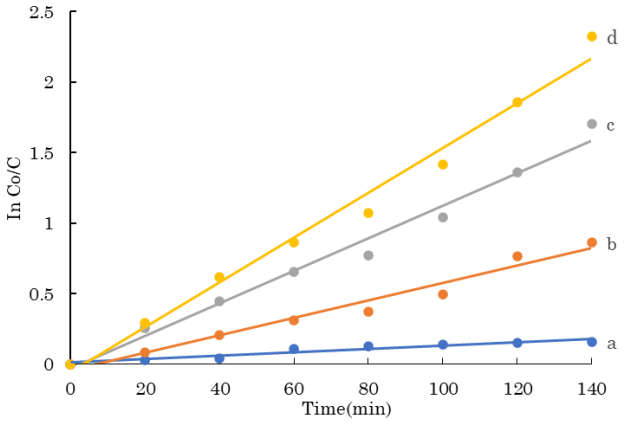

Figure 9. Fitted curves of the experimental data using a pseudo-first order kinetics equation during the photodegradation of methylene blue using (a) acrylics (b) TiO_2-acrylics, (c) TS-acrylics, and (d) TS-PANI-acrylics.

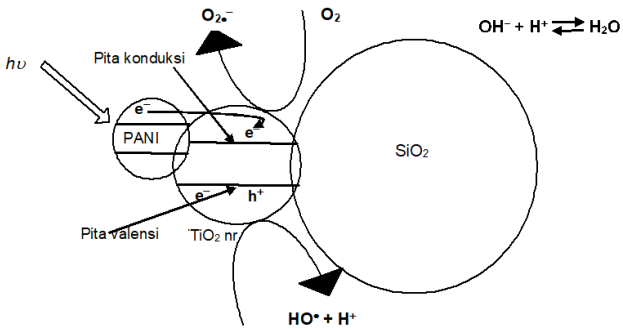

Figure 10. A plausible mechanism during photocatalytic degradation of MB solution using TS composites in the presence of PANI.

Table 4. Kinetics data of decreasing MB concentration by the coating composites.

Photocatalysts	k (min^{-1})	R^2	degradation of MB (%)	Adsorbed MB in 20 min (%)
acrylics	0.0012	0.9258	14.68	3.18
TiO_2-acrylics	0.0062	0.9691	57.80	8.11
TS-acrylics	0.0115	0.9822	81.83	22.67
TS-PANI-acrylics	0.0159	0.9845	90.22	25.54

composites to prevent the growth of foulant such as barnacles or other species at the surface of ship body that stopped at a beach or a port.

3.6 Anti-Fouling Test

Two main activities contributed to the anti-fouling activity of this coating. The first is the photocatalytic activity due to the composite content in the coating material (binder). On the other hand, the hydrophobic nature of the coating due to the nano-roughness texture of the surface. The surface topography of the coating identified through AFM images as is presented in Figure 11. Figure 11 presents the AFM image on the surface that showed fluctuations between hills and valleys

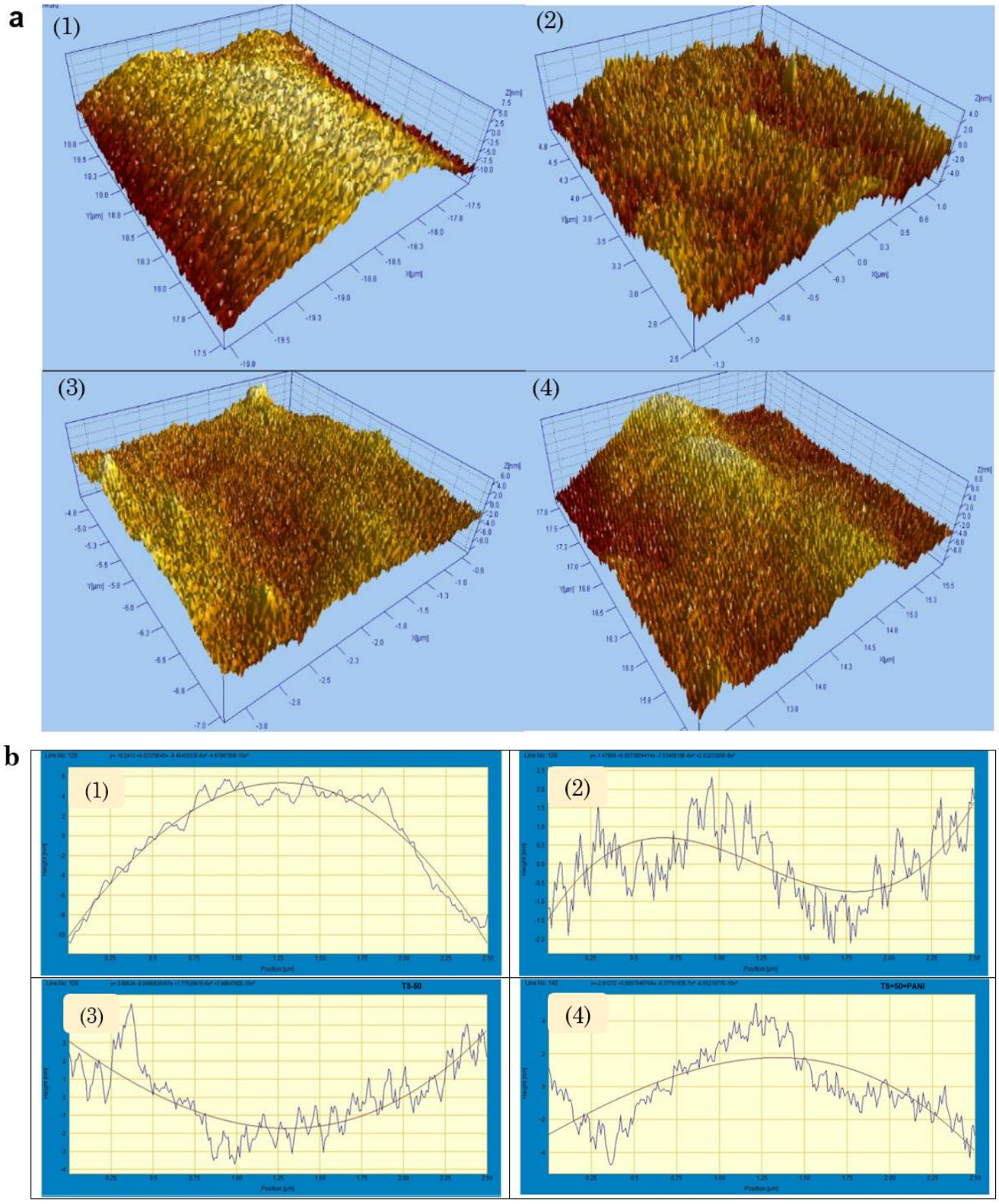

Figure 11. (a) The three-dimensional AFM images and (b) surface profiles of nano-roughness of 1) acrylic resin, 2) TiO_2-acrylic, 3) TS-acrylic, 4) TS-PANI-acrylic.

on the surface of the coating. The coating roughness profile of all analyzed samples shown in Figure 11a. The roughness profile noticeably of many hills and valleys on the surface also the steepness. In blank samples (only acrylic coating), some hills and valleys were not steep and tended to be flat. At the width of the same field, which was about 2.5 μm, the AFM images showed that the height of the hill on the surface of the acrylic coating was only about 16 nm. In contrast, on the nanorod TiO_2-acrylic coating appeared one hill and one valley with a considerable amount of roughness. There were more small hills and valleys in one profile at 2.5 μm width with a hill or valley height of about 4.5 nm.

The height of hills and valleys on the image of the TS-acrylic coating and the TS-PANI-acrylic coating were only about 8-9 nm. The surface topography was predicted by observing its roughness, wave amplitude (the presence of hills and valleys), distance, namely the distance between the roughness of the texture [60]. Figure 11b illustrates the nano-roughness profile on the coating surface based on AFM analysis. The nano-roughness of the surface was predicted through the model that commonly used, namely the average roughness (Ra). The Ra value indicates a natural roughness texture; the smaller the value, the better the nano-roughness. In this study, acrylic coating samples showed the Ra value of 10.27. The roughness in the TS-PANI-acrylic coating was 4.73, while in the TS-acrylic coating was 3.07. The smallest roughness was shown by the nanorod TiO_2 acrylic coating with the Ra value of 1.49.

The anti-fouling activity was evaluated by monitoring the growth of barnacles by immersing composite coated plates at Tanjung Emas Port for two months. The result showed the best anti-fouling performance in TS-PANI-acrylic composite coatings compared to others, as is shown in Figure 12. In this coating, there was almost no growth of barnacles for two months immersion at Tanjung Emas Port, Semarang.

4. Conclusions

TiO_2 nanorods have been developed as a photocatalyst for methylene blue degradation and as an anti-fouling agent in a coating. Efforts to improve the characteristics of TiO_2 provides the following results: the S_{BET} increased by 25% after being composited with SiO_2, i.e., from 64 m^2/g (TiO_2 nanorods) to 80.4 m^2/g (TS), and then increased more after coated by PANI (256.8 m^2/g). The photocatalytic activity increased by about 32% in TS composites compared to nanorod TiO_2. However, the photocatalytic activity of TS-PANI composite both on powder form and the coating only increased by about 6.5 % compared to TS-composite. This study showed that the nano-roughness factor also affected the performance of anti-fouling of the composites in addition to the photo-response factor of the composite. The surface roughness was probably due to the rod morphology of TiO_2, which could form excellent roughness on the surface. The topography of the surface reveal that the nano-roughness on the surface contributed additionally to the prevention of the attachment of fouling (barnacles).

As a photocatalyst, the TS-PANI composite showed a similar activity to the TS composite. As an anti-fouling material, the TS-PANI-acrylic composite coating was better than the TS-acrylic composite coating, which was shown by the less barnacle growth for two months immersion at Tanjung Emas Port, Semarang, Central Java, Indonesia. Therefore, TiO_2 nanorods, TS composite, and TS-PANI composites showed the potential to be developed as an environmentally friendly anti-fouling material.

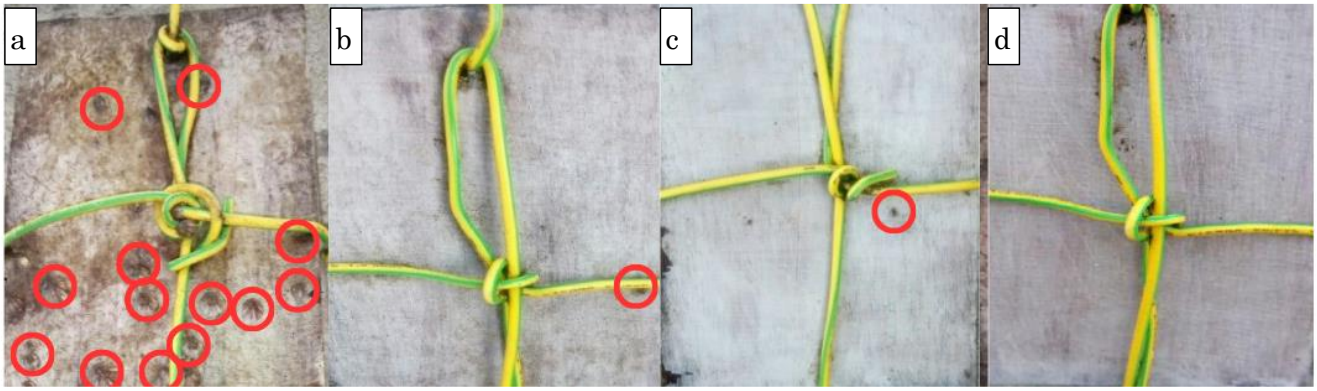

Figure 12. The photos of anti-fouling test on the plates coated by: (a) acrylic, (b) TiO_2-acrylic, (c) TS-acrylic, (d) TS-PANI-acrylic. (Note: The red circles indicated the growth of barnacles on the wood coated by acrylic without the use of TiO_2 composites.)

Acknowledgments

The authors would like thank Ms. N.D. Amalina (Pharmacy Study Program, Faculty of Medicine, Universitas Negeri Semarang) and Mr. R. Prasetyo (Laboratory of Chemistry, Universitas Negeri Semarang) for the helpful discussion during the manuscript writing and data presentation.

Credit Author Statement

Author Contributions: *S. Wahyuni*: Conceptualization, Methodology, Investigation, Resources, Data Curation, Writing Draft Preparation; *I. Kartini*: Conceptualization, Methodology, Formal Analysis, Data Curation, Visualization, Software, Review and Editing, Supervision; *S. Kadarwati*: Project Administration, Writing, Review and Editing, Data Validation. All authors have read and agreed to the published version of the manuscript.

References

[1] Mouni, L., Belkhiri, L., Bollinger, J.-C., Bouzaza, A., Assadi, A., Tirri, A., Dahmoune, F., Madani, K., Remini, H. (2018). Removal of methylene blue from aqueous solutions by adsorption on kaolin: kinetic and equilibrium studies. *Applied Clay Science,* 153, 38-45. DOI: 10.1016/j.clay.2017.11.034.

[2] El-Bery, H.M., Saleh, M., El-Gendy, R.A., Saleh, M.R., Thabet, S.M. (2022). High adsorption capacity of phenol and methylene blue using activated carbon derived from lignocellulosic agriculture wastes. *Scientific Reports,* 12, 5499. DOI: 10.1038/s41598-022-09475-4.

[3] Anushree, C., Philip, J. (2019). Efficient removal of methylene blue dye using cellulose capped Fe_3O_4 nanofluids prepared using oxidation-precipitation method. *Colloids and Surfaces A: Physicochemical and Engineering Aspects*, 567, 193-204. DOI: 10.1016/j.colsurfa.2019.01.057.

[4] Ihaddaden, S., Aberkane, D., Boukerroui, A., Robert, D. (2022). Removal of methylene blue (basic dye) by coagulation-flocculation with biomaterials (bentonite and *Opuntia ficus indica*). *Journal of Water Process Engineering*, 49, 102952. DOI: 10.1016/j.jwpe.2022.102952.

[5] Oyarce, E., Butter, B., Santander, P., Sánchez, J. (2021). Polyelectrolytes applied to remove methylene blue and methyl orange dyes from water via polymer-enhanced ultrafiltration. *Journal of Environmental Chemical Engineering*, 9, 106297. DOI: 10.1016/j.jece.2021.106297.

[6] Naffeti, M., Zaïbi, M.A., Nefzi, C., García-Arias, A.V., Chtourou, R., Postigo, P.A. (2023). Highly efficient photodegradation of methylene blue by a composite photocatalyst of bismuth nanoparticles on silicon nanowires. *Environmental Technology and Innovation*, 30, 103133. DOI: 10.1016/j.eti.2023.103133.

[7] Fujishima, A., Zhang, X. (2006). Titanium dioxide photocatalysis: present situation and future approaches. *Comptes Rendus Chimie,* 9(5–6), 750–760. DOI: 10.1016/j.crci.2005.02.055.

[8] Fujishima, A., Zhang, X., Tryk, D.A. (2007). Heterogeneous photocatalysis: From water photolysis to applications in environmental cleanup. *International Journal of Hydrogen Energy,* 32 (14), 2664-2672. DOI: 10.1016/j.ijhydene.2006.09.009.

[9] Schneider, J., Matsuoka, M., Takeuchi, M., Zhang, J., Horiuchi, Y., Anpo, M., Bahnemann, D.W. (2014). Understanding TiO_2 photocatalysis: mechanisms and materials. *Chemical Reviews,* 114(19), 9919-9986. DOI: 10.1021/cr5001892.

[10] Nakata, K., Fujishima, A. (2012). TiO_2 photocatalysis: Design and applications. *Journal of Photochemistry and Photobiology C: Photochemistry Reviews,* 13, 169-189. DOI: 10.1016/j.jphotochemrev.2012.06.001.

[11] Etacheri, V., Di Valentin, C., Schneider, J., Bahnemann, D., Pillai, S.C. (2015). Visible-light activation of TiO2 photocatalysts: Advances in theory and experiments. *Journal of Photochemistry and Photobiology C: Photochemistry Reviews,* 25, 1-29. DOI: 10.1016/j.jphotochemrev.2015.08.003.

[12] Chemin, J.B., Bulou, S., Baba, K., Fontaine, C., Sindzingre, T., Boscher, N.D., Choquet, P. (2018). Transparent anti-fogging and self-cleaning TiO_2/SiO_2 thin films on polymer substrates using atmospheric plasma. *Scientific Reports,* 8(1), 1-8. DOI: 10.1038/s41598-018-27526-7.

[13] Zhang, X., Guo, Y., Zhang, Z., Zhang, P. (2013). Self-cleaning superhydrophobic surface based on titanium dioxide nanowires combined with polydimethylsiloxane. *Applications of Surface Science,* 284, 319-323. DOI: 10.1016/j.apsusc.2013.07.100.

[14] Kallio, T., Alajoki, S., Pore, V., Ritala, M., Laine, J., Leskela, M., Stenius, P. (2006). Antifouling properties of TiO_2: Photocatalytic decomposition and adhesion of fatty and rosin acids, sterols and lipophilic wood extractives. *Colloids and Surfaces A: Physicochemical and Engineering Aspects,* 291 (1-3), 162-176. DOI: 10.1016/j.colsurfa.2006.06.044.

[15] Ruffolo, S.A., Macchia, A., La Russa, M.F., Mazza, L., Urzi, C., De Leo, F., Barberio, M., Crisci, G.M. (2013). Marine antifouling for underwater archaeological sites: TiO_2 and Ag-doped TiO_2. *International Journal of Photoenergy,* 2013, 251647. DOI: 10.1155/2013/251647.

[16] Cao, S., Wang, J.D., Chen, H.S., Chen, D.R. (2011). Progress of marine biofouling and antifouling technologies. *Chinese Science Bulletin,* 56(7), 598-612. DOI: 10.1007/s11434-010-4158-4.

[17] Mirabedini, A., Mirabedini, S.M., Babalou, A.A., Pazokifard, S. (2011). Synthesis, characterization and enhanced photocatalytic activity of TiO_2/SiO_2 nanocomposite in an aqueous solution and acrylic-based coatings. *Progress in Organic Coatings,* 72(3), 453-460. DOI: 10.1016/j.porgcoat.2011.06.002.

[18] Pazokifard, S., Esfandeh, M., Mirabedini, S.M. (2014). Photocatalytic activity of water-based acrylic coatings containing fluorosilane treated TiO_2 nanoparticles. *Progress in Organic Coatings,* 77(8), 1325-1335. DOI: 10.1016/j.porgcoat.2014.04.010.

[19] Lin, Y., Li, D., Hu, J., Xiao, G., Wang, J., Li, W., Fu, X. (2012). Highly efficient photocatalytic degradation of organic pollutants by PANI-modified TiO_2 composite. *Journal of Physical Chemistry C,* 116(9), 5764-5772. DOI: 10.1021/jp211222w.

[20] Mostafaei, A., Nasirpouri, F. (2013). Preparation and characterization of a novel conducting nanocomposite blended with epoxy coating for antifouling and antibacterial applications. *Journal of Coatings Technology and Research,* 10(5), 679-694. DOI: 10.1007/s11998-013-9487-1.

[21] Xu, C., Fang, L., Huang, Q., Yin, B., Ruan, H., Li, D. (2013). Preparation and characterization of a novel conducting nanocomposite blended with epoxy coating for antifouling and antibacterial applications. *Thin Solid Films,* 531, 255-260. DOI: 10.1016/j.tsf.2012.12.039.

[22] Li, Y., Yu, Y., Wu, L., Zhi, J. (2013). Processable polyaniline/titania nanocomposites with good photocatalytic and conductivity properties prepared via peroxo-titanium complex catalyzed emulsion polymerization approach. *Applied Surface Science,* 273, 135-143. DOI: 10.1016/j.apsusc.2013.01.213.

[23] Ohno, T., Numakura, K., Itoh, H., Suzuki, H., Matsuda, T. (2009). Control of the quantum size effect of TiO_2-SiO_2 hybrid particles. *Materials Letters,* 63(20), 1737-1739. DOI: 10.1016/j.matlet.2009.05.032.

[24] Joo, J.B., Lee, I., Dahl, M., Moon, G.D., Zaera, F., Yin, Y. (2013). Controllable synthesis of mesoporous TiO_2 hollow shells: toward an efficient photocatalyst. *Advanced Functional Materials,* 23(34), 4246-4254. DOI: 10.1002/adfm.201300255.

[25] Joo, J.B., Zhang, Q., Lee, I., Dahl, M., Zaera, F., Yin, Y. (2012). Mesoporous anatase titania hollow nanostructures though silica-protected calcination. *Advanced Functional Materials*, 22(1), 166-174. DOI: 10.1002/adfm.201101927.

[26] Chen, M.L., Qu, Y.Y., Yang, L., Gao, H. (2008). Mesoporous anatase titania hollow nanostructures though silica-protected calcination. *Science China Chemistry,* 51(9), 848-852. DOI: 10.1007/s11426-008-0069-5.

[27] Wei, Z., Zhang, Q., Liu, Y., Xiong, R., Pan, C., Shi, J. (2011). Synthesis and photocatalytic activity of polyaniline-TiO_2 composites with bionic nanopapilla structure. *Journal of Nanoparticle Research,* 13, 3157–3165. DOI: 10.1007/s11051-010-0212-z.

[28] Zhang, Q., Lee, I., Joo, J.B., Zaera, F., Yin, Y. (2013). Core–shell nanostructured catalysts. *Accounts of Chemical Research,* 46(8), 1816–1824. DOI: 10.1021/ar300230s.

[29] Hashemi-Nasab, R., Mirabedini, S.M. (2013). Effect of silica nanoparticles surface treatment on in situ polymerization of styrene-butyl acrylate latex. *Progress in Organic Coatings,* 76(7-8), 1016-1023. DOI: 10.1016/j.porgcoat.2013.02.016.

[30] Li, X., Wang, D., Cheng, G., Luo, Q., An, J., Wang, Y. (2008). Preparation of polyaniline-modified TiO_2 nanoparticles and their photocatalytic activity under visible light illumination. *Applied Catalysis B: Environmental,* 81, 267-273. DOI: 10.1016/j.apcatb.2007.12.022.

[31] Wang, F., Min, S., Han, Y., Feng, L. (2010). Visible-light-induced photocatalytic degradation of methylene blue with polyaniline-sensitized TiO_2 composite photocatalysts. *Superlattices and Microstructures,* 48(2), 170-180. DOI: 10.1016/j.spmi.2010.06.009.

[32] Kim, B.S., Lee, K.T., Huh, P.H., Lee, D.H., Jo, N.J., Lee, J.O. (2009). In situ template polymerization of aniline on the surface of negatively charged TiO_2 nanoparticles. *Synthetic Metals,* 159, 1369-1372. DOI: 10.1016/j.synthmet.2009.03.012.

[33] Xu, S., Jiang, L., Yang, H., Song, Y., Dan, Y. (2011). In situ template polymerization of aniline on the surface of negatively charged TiO_2 nanoparticles. *Chinese Journal of Catalysis,* 32(3-4), 536-545. DOI: 10.1016/s1872-2067(10)60207-0.

[34] Deivanayaki, S., Ponnuswamy, V., Mariappan, R., Jayamurugan, P. (2013). Synthesis and characterization of polypyrrole/TiO_2 composites by chemical oxidative method. *Optik,* 124(12), 1089-1091. DOI: 10.1016/j.ijleo.2012.02.029.

[35] Dimitrijevic, N.M., Tepavcevic, S., Liu, Y., Rajh, T., Silver, S.C., Tiede, D.M. (2013). Nanostructured TiO_2/polypyrrole for visible light photocatalysis. *The Journal of Physical Chemistry C,* 117(30), 15540–15544. DOI: 10.1021/jp405562b.

[36] Wahyuni, S., Kunarti, E.S., Swasono, R.T., Kartini, I. (2018). Characterization and photocatalytic activity of TiO_2 (rod)-SiO_2-polyaniline nanocomposite. *Indonesian Journal of Chemistry,* 18(2), 321-330. DOI: 10.22146/ijc.22550.

[37] Christy, P.D., Melikechi, N., Nirmala Jothi, N.S., Suganthi, A.R.B., Sagayaraj, P. (2010). Synthesis of TiO_2 nanorods by oriented attachment using EDTA modifier: A novel approach towards 1D nanostructure development. *Journal of Nanparticle Research,* 12(8), 2875-2882. DOI: 10.1007/s11051-010-9877-6.

[38] Rahman, I.A., Padavettan, V. (2012). Synthesis of Silica nanoparticles by sol-gel: Size-dependent properties, surface modification, and applications in silica-polymer nanocomposites: a review. *Journal of Nanomaterials,* 2012, 1-15. DOI: 10.1155/2012/132424.

[39] Wilhelm, P., Stephan, D. (2006). On-line tracking of the coating of nanoscaled silica with titania nanoparticles via zeta-potential measurements. *Journal of Colloid and Interface Science,* 293(1), 88-92. DOI: 10.1016/j.jcis.2005.06.047.

[40] Fu, G., Vary, P.S., Lin, C.-T. (2005). Anatase TiO_2 nanocomposites for antimicrobial coatings. *Journal of Physical Chemistry B,* 109(IV), 8889-8898. DOI: 10.1021/jp0502196.

[41] Zuccheri, T., Colonna, M., Stefanini, I., Santini, C., Di Gioia, D. (2013). Bactericidal activity of aqueous acrylic paint dispersion for wooden substrates based on TiO_2 nanoparticles activated by fluorescent light. *Materials (Basel),* 6(8), 3270-3283. DOI: 10.3390/ma6083270.

[42] Baek, I.C., Vithal, M., Chang, J.A.,Yum, J-H., Nazeeruddin, Md.K., Gratzel, M., Chung, Y-C., Seok, S.I. (2009). Facile preparation of large aspect ratio ellipsoidal anatase TiO_2 nanoparticles and their application to dye-sensitized solar cell. *Electrochemistry Communications,* 11(4), 909-912. DOI: 10.1016/j.elecom.2009.02.026.

[43] Chemseddine, A., Moritz, T. (1999). Nanostructuring titania: control over nanocrystal structure, size, shape, and organization. *European Journal of Inorganic Chemistry,* 1999(2), 235-245. DOI: 10.1002/(SICI)1099-0682(19990202)1999:2<235::AID-EJIC235>3.0.CO;2-N.

[44] Ilican, S., Caglar, Y., Caglar, M., Demirci, B. (2008). Polycrystalline indium-doped ZnO thin films: preparation and characterization. *Journal of Optoelectronics and Advanced Materials,* 10(10), 2592-2598.

[45] Sadhu, S., Poddar, P. (2014). Template-free fabrication of highly-oriented single-crystalline 1D-rutile TiO_2-MWCNT composite for enhanced photoelectrochemical activity. *Journal of Physical Chemistry C*, 118(33), 19363-19373. DOI: 10.1021/jp5023983.

[46] Singh, A., Vishwakarma, H.L. (2015). Study of structural, morphological, optical and electroluminescent properties of undoped ZnO nanorods grown by a simple chemical precipitation. *Materials Science-Poland,* 33(4), 751-759. DOI: 10.1515/msp-2015-0112.

[47] Solís-Pomar, F., Martínez, E., Meléndrez, M.F., Pérez-Tijerina, E. (2011). Growth of vertically aligned ZnO nanorods using textured ZnO films. *Nanoscale Research Letters,* 6(1), 1-11. DOI: 10.1186/1556-276X-6-524.

[48] Thommes, M., Kaneko, K., Neimark, A.V., Olivier, J.P., Rodriguez-Reinoso, F., Rouquerol, J., Sing, K.S.W. (2015). Physisorption of gases, with special reference to the evaluation of surface area and pore size distribution (IUPAC Technical Report). *Pure and Applied Chemistry,* 87(9-10), 1051-1069. DOI: 10.1515/pac-2014-1117.

[49] Donohue, M.D., Aranovich, G.L. (1998). Adsorption hysteresis in porous solids. *Journal of Colloid and Interface Science,* 205(1), 121-130. DOI: 10.1006/jcis.1998.5639.

[50] Carja, G., Nakamura, R., Aida, T., Niiyama, H. (2001). Textural properties of layered double hydroxides: effect of magnesium substitution by copper or iron. *Microporous and Mesoporous Materials,* 47(2-3), 275-284. DOI: 10.1016/S1387-1811(01)00387-0.

[51] Fan, H., Do, D.D., Nicholson, D. (2013). Condensation and evaporation in capillaries with nonuniform cross sections. *Industrial and Engineering Chemistry Research*, 52(39), 14304-14314. DOI: 10.1021/ie402549z.

[52] Wagner, C.D., Riggs, W.M., Davis, L.E., Moulder, J.F., Muilenberg, G.E. (1979). *Handbook of X ray photoelectron spectroscopy–a reference book of standard spectra for identification and interpretation*. Minnesota: Perkin Elmer Corporation.

[53] Silversmit, G., De Doncker, G., De Gryse, R. (2002). A mineral TiO_2(001) anatase crystal examined by XPS. *Surface Science Spectra,* 9(1), 21-29. DOI: 10.1116/11.20020701.

[54] Krishnan, P., Liu, M., Itty, P.A., Liu, Z., Rheinheimer, V., Zhang, M-H., Monteiro, P.J.M., Yu, L.E. (2017). Characterization of photocatalytic TiO_2 powder under varied environments using near ambient pressure X-ray photoelectron spectroscopy. *Scientific Reports,* 7, 43298-43309. DOI: 10.1038/srep43298.

[55] Wang, D.P., Zeng, H.C. (2009). Multifunctional roles of TiO_2 nanoparticles for architecture of complex core-shells and hollow spheres of SiO_2–TiO_2–polyaniline system. *Chemistry of Materials,* 21(20), 4811-4823. DOI: 10.1021/cm901509t.

[56] Kang, E. (1998). Polyaniline: A polymer with many interesting intrinsic redox states. *Progress in Polymer Science,* 23(97), 277-324. DOI: 10.1016/S0079-6700(97)00030-0.

[57] Wu, C.-G., Chen, J.-Y. (1997). Chemical deposition of ordered conducting polyaniline film via molecular self-assembly. *Chemistry of Materials*, 9(2), 399-402. DOI: 10.1021/cm9602860.

[58] Huang, X., Wang, G., Yang, M., Guo, W., Gao, H. (2011). Synthesis of polyaniline-modified $Fe_3O_4/SiO_2/TiO_2$ composite microspheres and their photocatalytic application. *Materials Letters,* 65(19-20), 2887-2890. DOI: 10.1016/j.matlet.2011.06.005.

[59] Liu, Z., Miao, Y.-E., Liu, M., Ding, Q., Tjiu, W.W., Cui, X., Liu, T. (2014). Flexible polyaniline-coated TiO_2/SiO_2 nanofiber membranes with enhanced visible-light photocatalytic degradation performance. *Journal of Colloid Interface Science*, 424, 49-55. DOI: 10.1016/j.jcis.2014.03.009.

[60] Bellitto, V. (Ed.). (2012). *Atomic force microscopy – imaging, measuring and manipulating surfaces at the atomic scale*. In Tech. DOI: 10.5772/2673.